EPTT 2024
Escola de Primavera de Transição e Turbulência

ABCM
Associação Brasileira de Engenharia e Ciências Mecânicas

EPTT-2024-0057
Resolvent-based analysis of near-wall coherent structures in turbulent boundary layer

Felipe Pinheiro
Denilso Paulo Souza dos Santos
Leandra Isabel de Abreu
São Paulo State University (UNESP), School of Engineering - Campus of São João da Boa Vista
felipe.pinheiro@unesp.br
denilson.santos@unesp.br
leandra.abreu@unesp.br

Abstract. *Resolvent-based analysis combined with Spectral Proper Orthogonal Decomposition (SPOD) provides a robust framework for understanding near-wall coherent structures in turbulent boundary layers. This study focuses on the low- and high-frequency interactions that shape the dynamics of these structures. Resolvent analysis, grounded in linearized Navier-Stokes equations, identifies key flow structures by treating nonlinear terms as a forcing mechanism, while SPOD decomposes the turbulent flow into energy-optimal modes. By applying these methods to boundary layer data, we uncover dominant coherent structures responsible for energy transfer and momentum transport. The results demonstrate how resolvent modes correlate with SPOD modes, offering insights into the spatio-temporal behavior of near-wall turbulence. These findings enhance our understanding of wall-bounded turbulence mechanisms and offer potential pathways for turbulence control strategies.*

Keywords: *Resolvent analysis, turbulent boundary layer, SPOD, DNS*

1. INTRODUCTION

Understanding the dynamics of near-wall coherent structures in turbulent boundary layers is critical for improving predictions of skin friction, heat transfer, and drag, which are essential for various engineering applications, including aerospace and energy systems. Despite significant progress in the field of turbulence research, the underlying mechanisms responsible for the formation, maintenance, and interaction of these structures remain complex and elusive (Abreu *et al.*, 2019). Near-wall turbulence is characterized by the presence of self-sustaining structures such as streaks and vortices, which dominate momentum and energy transfer. A detailed understanding of these structures and their dynamics can potentially lead to more effective turbulence control strategies, improving efficiency in practical systems.

One promising approach for studying such complex flow phenomena is resolvent analysis, a framework derived from the linearized Navier-Stokes equations (McKeon, 2017; Towne *et al.*, 2018). In this formulation, the nonlinear components of the flow are treated as an external forcing, and the system's response is analyzed as a linear amplification problem. This approach provides insight into the most amplified flow structures, which often correspond to coherent structures observed in the turbulent boundary layer. Resolvent analysis identifies the forcing-response pairs that dominate the system's behavior, making it a powerful tool for dissecting the dynamics of turbulence.

To complement resolvent analysis, Spectral Proper Orthogonal Decomposition (SPOD) is employed to extract energy-optimal modes from the turbulent flow field (Abreu *et al.*, 2017; Towne *et al.*, 2018). SPOD, a data-driven technique, identifies spatial structures associated with specific frequency bands, making it ideal for decomposing the flow into coherent structures across a wide range of scales. By combining resolvent analysis with SPOD, we aim to bridge the gap between theoretical predictions and empirical observations, offering a comprehensive view of near-wall turbulence.

This paper investigates the interaction between resolvent and SPOD modes in the context of a turbulent boundary layers. Specifically, we focus on the near-wall region where turbulent production and dissipation are most intense. Through this analysis, we seek to identify key flow structures that govern the dynamics of near-wall turbulence and provide a deeper understanding of their role in energy transport and momentum transfer. The insights gained from this study may also contribute to the development of novel strategies for turbulence modeling and control.

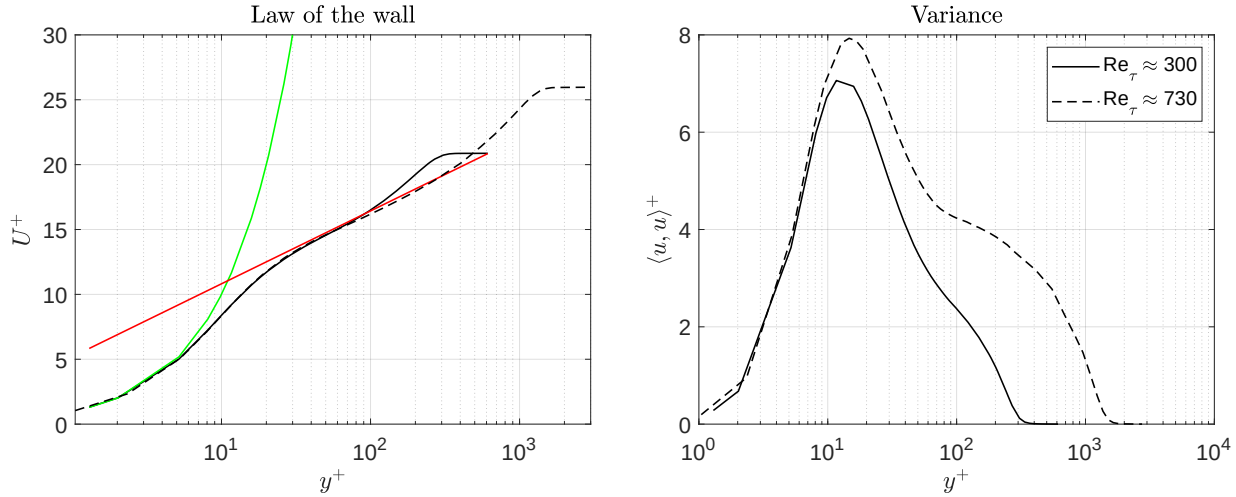

Figure 1. Turbulence statistics of the zero-pressure-gradient turbulent boundary layer (Eitel-Amor *et al.*, 2014) showing (a) the mean streamwise velocity profiles and (b) the variance of the streamwise velocity fluctuations at $Re_\tau \approx 300$ (black solid line) and 730 (black dashed line), both scaled in viscous units. In (a) the green solid line represents the linear law, $\bar{u}^+ = y^+$; and the red solid line is the log law, $\bar{u}^+ = (1/\kappa)\ln y^+ + B$, where $\kappa = 0.41$ and $B = 5.2$.

2. Database description

The large-eddy simulation (LES) database employed in this work were produced in Eitel-Amor *et al.* (2014) for a zero-pressure-gradient turbulent boundary layer. The corresponding Reynolds numbers based in inner units are $Re_\tau \approx 300$ and 730, respectively.

2.1 Turbulence statistics and spectral analysis

Using standard Reynolds decomposition and considering velocity in inner units, $\mathbf{u}^+ = \bar{\mathbf{u}}^+ + \mathbf{u}'^+$, the mean streamwise velocity profiles $\bar{\mathbf{u}}^+$ and the variance profiles of the streamwise velocity fluctuations $\overline{(\mathbf{u}'^+)^2}$ are shown in Figures 1 (a) and (b) respectively, for the turbulent boundary layer database (Eitel-Amor *et al.*, 2014), for the friction Reynolds numbers $Re_\tau \approx 300$ and 730. The mean velocity profiles exhibit the characteristic form typical of wall-bounded turbulent flows when plotted against the wall distance scaled by inner variables y^+, following the linear and log laws (Millikan, 1938; Marusic *et al.*, 2013). The variance profiles display the typical pattern found in wall-bounded turbulent flows, featuring a peak near the wall in the buffer layer at $y^+ \approx 15$. This peak becomes more pronounced as the Reynolds number increases, as expected (Eitel-Amor *et al.*, 2014; Monkewitz and Nagib, 2015).

To examine the turbulent structures found in the buffer layer, Figure 2 shows the two-dimensional inner-scaled pre-multiplied power-spectral density of streamwise velocity fluctuations $k_z E^+_{uu}$ for $Re_\tau \approx 300$ and 730, where k_z refer respectively to cross-streamwise wavenumber. For both Reynolds numbers, the results show a highly energetic peak located near the wall for the wavelength combination $(y^+, \lambda_z^+) \approx (100, 100)$. This combination of wavelengths characterizes the typical pattern of the near-wall cycle, consisting of streaks and streamwise vortices, a phenomenon that has been widely examined in numerous studies across various Reynolds numbers and flow conditions (see for instance Refs. Hoyas and Jiménez (2006); Monty *et al.* (2009); Smits *et al.* (2011)).

3. Mathematical model

3.1 SPOD

The present SPOD was employed following the procedure outlined in Ref. Towne *et al.* (2018). In the present study, SPOD is applied to the velocity fluctuations $\mathbf{q}' = [\mathbf{u}', \mathbf{v}', \mathbf{w}']$ to extract orthogonal modes that optimally represent turbulent kinetic energy. We first perform a Fourier transform in time to obtain the field for a specifc frequency ω. For the present case the DNS uses periodic boundary conditions in the x and z directions, which are homogeneous and therefore Fourier modes become optimal. Thus, we also perform a Fourier decomposition in the x and z directions to obtain a field for specific streamwise and spanwise wavenumbers.

Once we have the transformed field for a specific frequency-wavenumber combination, $\hat{\mathbf{q}}' = \hat{\mathbf{q}}'(k_x, y, k_z, \omega)$, where hats denote Fourier-transformed quantities and $\hat{\mathbf{q}}' = [\hat{\mathbf{u}}', \hat{\mathbf{v}}', \hat{\mathbf{w}}']$ are the state variables, it is possible to apply the SPOD

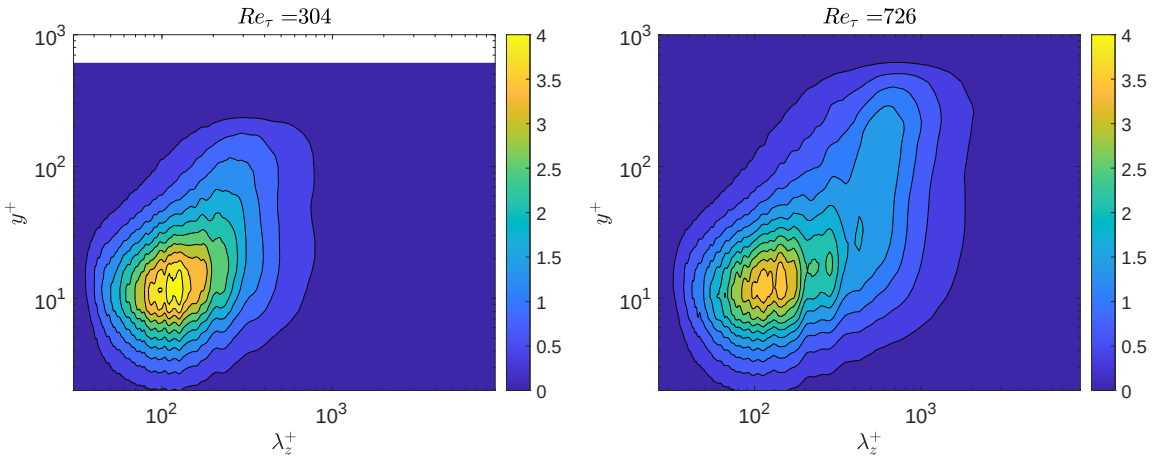

Figure 2. Two-dimensional inner-scaled premultiplied power-spectral density of the streamwise velocity $k_z E_{uu}^+$, at $y^+ \approx 15$, for the two Reynolds numbers under study.

to this transformed field, which is equivalent to solving the integral equation:

$$\int_{y'} \mathbf{C}(y, y')\Psi(y')\mathrm{d}y' = \lambda\Psi(y), \tag{1}$$

where Ψ are the SPOD modes, λ is the corresponding eigenvalue and $\mathbf{C}$ is the two-point cross-spectral density between the three velocity components, the dimension of which is $3N_y \times 3N_y$, where N_y is the number of points in the wall-normal coordinate. Note that $\mathbf{C}$ is Hermitian, thus eigenvalues are real and positive, and eigenfunctions are orthogonal. The eigenvalues are arranged in descending order, ensuring that the modes with the highest kinetic energy come first. As a result, the leading modes correspond to large-scale flow structures.

3.2 Resolvent Analysis

In turbulent flow, the Navier-Stokes equations can be divided into linear and nonlinear components related to flow fluctuations. The linear terms are derived by linearizing the system around the mean velocity profile, which serves as the base flow. The nonlinear terms are treated as external forcing, and resolvent analysis focuses on identifying the forcings that most effectively drive the linearized flow responses. In this study, we have used the mean flow averaged over all homogeneous directions as the base flow, shown in Figure 1 (a) for the channel flow at both Reynolds numbers, to linearise the Navier–Stokes equations.Since the system is time-invariant, all quantities in the Navier-Stokes equations can be decomposed using a Fourier transform in time, resulting in a problem formulated in the frequency domain. This approach follows the methodology outlined in Ref. Cavalieri *et al.* (2019) we can rearrange the equations, leading to the linearised Navier–Stokes system in the input-output form:

$$\hat{\mathbf{q}}' = \mathcal{R}\mathbf{f}, \tag{2}$$

where $\mathbf{f} = [\mathbf{f_x}, \mathbf{f_y}, \mathbf{f_z}]$ is the input, or resolvent forcing modes; $\hat{\mathbf{q}}' = [\hat{\mathbf{u}}', \hat{\mathbf{v}}', \hat{\mathbf{w}}']$ is the output of the selected flow variables, or associated response modes; and $\mathcal{R}$ is the resolvent operator.

The singular value decomposition of the resolvent operator, discretised as a matrix $\mathbf{R}$ leads to optimal forcing modes, causing maximum amplification between input and output,

$$\mathbf{R} = \mathbf{U}\mathbf{\Sigma}\mathbf{V}^\dagger, \tag{3}$$

where the superscript † denotes conjugate transpose of a matrix. The above equation decomposes $\mathbf{R}$ into two orthonormal bases $\mathbf{U} = [\mathbf{u_1}, \mathbf{u_2}, ..., \mathbf{u_n}]$ and $\mathbf{V} = [\mathbf{v_1}, \mathbf{v_2}, ..., \mathbf{v_m}]$, where n and m are the output and input dimensions, respectively. Note that $\mathbf{U}^\dagger\mathbf{U} = \mathbf{I}$ and $\mathbf{V}^\dagger\mathbf{V} = \mathbf{I}$. Here $\mathbf{U}$ and $\mathbf{V}$ are respectively output and input bases. The matrix $\mathbf{\Sigma}$ is diagonal, with real, positive values, in decreasing order $\sigma_1 \geq \sigma_2 \geq ... \geq \sigma_n$. If the forcing is $\mathbf{f} = \mathbf{v_1}$, the flow response is $\hat{\mathbf{q}}' = \sigma_1\mathbf{u_1}$, and since σ_1 is the maximum gain between input and output, $(\mathbf{u_1}, \mathbf{v_1})$ is thus the optimal forcing and associated response, which is the most amplified one.

4. Comparisons between SPOD and resolvent analysis

Figure 3 shows the comparisons between the first SPOD mode and the optimal response from resolvent analysis for (a) $Re_\tau \approx 300$ and (b) $Re_\tau \approx 730$. These comparisons highlight the effectiveness of resolvent analysis in capturing the

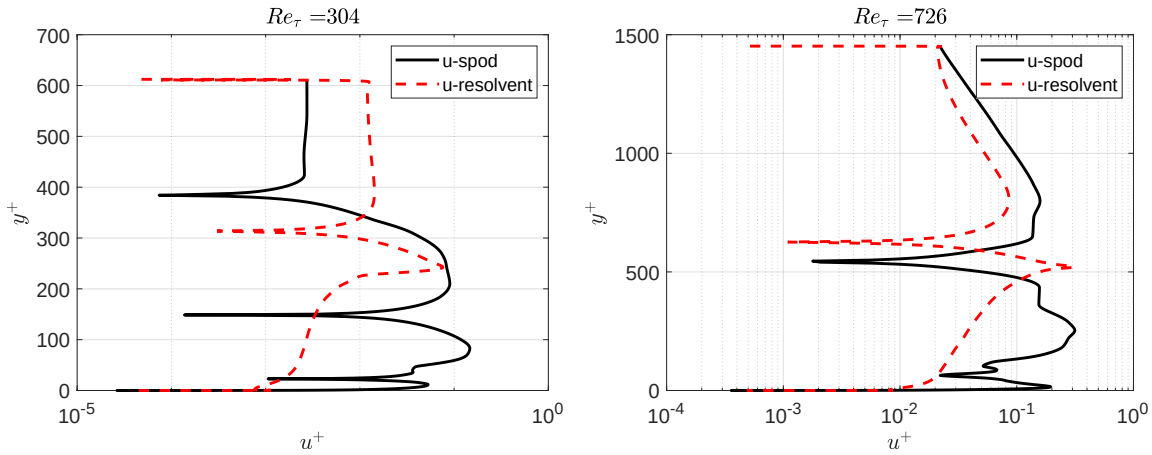

Figure 3. First SPOD mode (black solid line) compared with the response associated to the optimal forcing from resolvent analysis (red dashed line) for (a) $Re_\tau \approx 300$ and (b) $Re_\tau \approx 730$.

dominant structures in turbulent flows across different Reynolds numbers. At $Re_\tau \approx 300$, the optimal resolvent response closely matches the first SPOD mode, indicating a strong alignment between the linear amplification mechanisms predicted by resolvent analysis and the energy-optimal structures identified by SPOD. This suggests that for lower Reynolds numbers, the near-wall coherent structures are well captured by the leading resolvent mode, which corresponds to key flow features such as streaks and vortices that are central to the dynamics of near-wall turbulence.

At the higher Reynolds number, $Re_\tau \approx 730$, the comparison reveals more complex interactions. While there is still a notable similarity between the first SPOD mode and the optimal resolvent response, the higher Reynolds number introduces additional scales of motion and more intricate flow features. The first SPOD mode captures the dominant energetic structures, but the resolvent analysis identifies broader forcing-response interactions that may not be fully captured by a single mode. This suggests that as the Reynolds number increases, the flow becomes more multiscale, and additional resolvent modes might be needed to account for the full range of dynamics.

5. Conclusions

This work has shown that resolvent-based analysis can be effectively coupled with spectral proper orthogonal decomposition (SPOD) for studying near-wall coherent structures in turbulent boundary layers. Information from the resolvent analysis indicates the linear amplification mechanisms of coherent structures, while SPOD identifies modes optimally energetic at different frequencies, thus providing a fine filter between decomposed components of the dynamics. Results reveal a very good match of resolvent modes with SPOD modes, especially in the near-wall area, where streaks and vortices are important by being large convective structures carrying momentum and energy.

The analysis showed that resolvent modes capture the essential features of coherent structures driving turbulence production and its subsequent dissipation. The findings help contribute a refined insight into the self-organization of turbulent boundary layers sustaining near-wall turbulence. Moreover, this work highlights the potential of resolvent-based analysis and SPOD as complementary tools in modeling and predicting turbulence structures to fill the gap between theoretical and experimental observations.

The knowledge obtained from this research is the first step in further studies toward effective flow control strategies that reduce drag and improve aerodynamic performance. Enhancing our understanding of near-wall coherent structures and the mechanisms producing these structures paves the way for developing alternative strategies that are more efficient in controlling wall-bounded turbulence, in terms of practical applications.

6. ACKNOWLEDGEMENTS

The authors acknowledge the financial support received from the São Paulo Research Foundation, FAPESP, under process number 2023/01391-5, and the financial support from FINEP project under the reference number 0527/18.

7. REFERENCES

Abreu, L.I., Cavalieri, A.V.G. and Wolf, W.R., 2017. “Coherent hydrodynamic waves and trailing-edge noise”. In *23rd AIAA/CEAS Aeroacoustics Conference*. p. 3173.

Abreu, L.I., Nogueira, P.A., Nilton, M.M. and Cavalieri, A.V., 2019. “Resolvent analysis applied to acoustic analogies”. In *25th AIAA/CEAS Aeroacoustics Conference*. p. 2402.

Cavalieri, A., Jordan, P. and Lesshafft, L., 2019. "Wave-packet models for jet dynamics and sound radiation". *Applied Mechanics Reviews*, Vol. 71, No. 2, p. 020802.

Eitel-Amor, G., Örlü, R. and Schlatter, P., 2014. "Simulation and validation of a spatially evolving turbulent boundary layer up to $Re_\theta = 8300$". *International Journal of Heat and Fluid Flow*, Vol. 47, pp. 57–69.

Hoyas, S. and Jiménez, J., 2006. "Scaling of the velocity fluctuations in turbulent channels up to $Re_\tau = 2003$". *Physics of Fluids*, Vol. 18, No. 1, p. 011702.

Marusic, I., Monty, J.P., Hultmark, M. and Smits, A.J., 2013. "On the logarithmic region in wall turbulence". *Journal of Fluid Mechanics*, Vol. 716.

McKeon, B., 2017. "The engine behind (wall) turbulence: perspectives on scale interactions". *Journal of Fluid Mechanics*, Vol. 817, p. P1.

Millikan, C., 1938. "Proc. 5th int. cong. appl. mech." pp. 386–392.

Monkewitz, P.A. and Nagib, H.M., 2015. "Large-reynolds-number asymptotics of the streamwise normal stress in zero-pressure-gradient turbulent boundary layers". *Journal of Fluid Mechanics*, Vol. 783, pp. 474–503.

Monty, J., Hutchins, N., Ng, H., Marusic, I. and Chong, M., 2009. "A comparison of turbulent pipe, channel and boundary layer flows". *Journal of Fluid Mechanics*, Vol. 632, pp. 431–442.

Smits, A., McKeon, B. and Marusic, I., 2011. "High–Reynolds number wall turbulence". *Annual Review of Fluid Mechanics*, Vol. 43, pp. 353–375.

Towne, A., Schmidt, O.T. and Colonius, T., 2018. "Spectral proper orthogonal decomposition and its relationship to dynamic mode decomposition and resolvent analysis". *Journal of Fluid Mechanics*, Vol. 847, pp. 821–867.

8. RESPONSIBILITY NOTICE

The authors are the only responsible for the printed material included in this paper.